PERGAMON

International Journal of Solids and Structures 39 (2002) 3313–3336

INTERNATIONAL JOURNAL OF SOLIDS and STRUCTURES

www.elsevier.com/locate/ijsolstr

Buckling of steel bars with Lüders bands

Edmundo Corona [a,*], John A. Shaw [b], Mark A. Iadicola [b]

[a] *Department of Aerospace and Mechanical Engineering, 365 Fitzpatrick Hall, University of Notre Dame, Notre Dame, IN 46556–5637, USA*

[b] *Department of Aerospace Engineering, The University of Michigan, USA*

Received 2 October 2001; received in revised form 2 December 2001

Abstract

Experiments and simulations are presented for the study of interaction between material and structural instabilities that occur in mild steel bars under axial compression. The material instability consists of Lüders bands that nucleate and propagate along the specimens. The structural instability involves lateral deflections of the bar leading to collapse. The study includes an investigation of bars of several different lengths. The mechanical response in the experiments were monitored through measurements of axial load, axial and midspan lateral displacements, and full field imaging of a brittle coating showing the Lüders deformation. Interesting interactions exist between the localized deformation due to the material-level instabilities and the global collapse of the bars. Finite element simulations, using a constitutive model with a nonmonotonic stress–strain behavior, showed good agreement with the experiments and helped to explain the variety of collapse modes seen in the experiments. The symmetry of imperfections and/or loading misalignments have dramatic effects on the evolution of Lüders deformation and the eventual collapse mode. Certain imperfections lead to deformation modes that delay structural collapse.

Keywords: Buckling; Lüders bands; Column; Collapse; Instability

1. Introduction

In some engineering applications structural members are made of hot-finished steels that exhibit Lüders bands when loaded into the plastic range. Under stroke-controlled tension (or compression), such materials exhibit load–extension (F–δ) curves similar to the one shown in Fig. 1, characterized by a load plateau following initial yield. In this figure, the extension is normalized by the length of the specimen (L) while the load is divided by the cross-sectional area of the unloaded specimen (A). The initiation and propagation of Lüders bands in uniaxial tension experiments are well-known material instabilities (see the nice experimental study by Butler (1962) and the book by Hall (1970)). The mechanical aspects have been recently discussed in detail by Kyriakides and Miller (2000).

Here we provide a brief description of the phenomenon. Referring to Fig. 1, the specimen is initially unloaded at point ⓪. Between points ⓪ and ① the material is essentially linearly elastic and the deformation

* Corresponding author. Fax: +1-574-631-8341.
E-mail address: ecorona@nd.edu (E. Corona).

0020-7683/02/$ - see front matter
PII: S0020-7683(02)00156-7

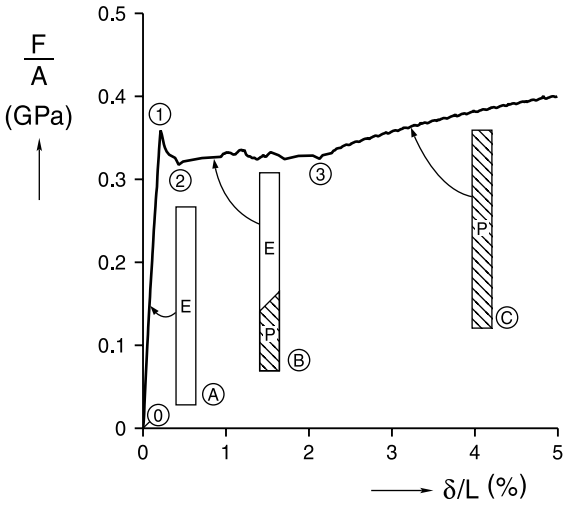

Fig. 1. Tensile force–displacement response of an AISI 1018 steel specimen that exhibits Lüders bands.

is homogeneous (insert Ⓐ). At point ① Lüders bands nucleate locally in the specimen and the load drops to point ②. Further stretching occurs at a relatively constant load due to the propagation of Lüders bands (insert Ⓑ). The deformation in the specimen is distinctly inhomogeneous at this time. The part of the specimen labeled E is linearly elastic, while the part labeled P has yielded. Under continued extension, the Lüders bands continue traversing the length of the specimen until the entire test section has yielded at point ③. The strain range of the load plateau is called the Lüders strain. Further stretching results in essentially homogeneous, strain-hardening, elastic–plastic deformation of the specimen. It is important to note that between points ② and ③, the strain in the elastic part of the specimen is given by F/EA where E is Young's modulus, while the strain in the plastic part has increased by the Lüders strain (the difference in δ/L between ③ and ①). It is also possible to have more than one Lüders band front propagating through the specimen. The number of fronts can be observed by proper visualization techniques. Only one front is shown in the figure for simplicity.

Lüders bands may also occur if the specimen is loaded in compression, but now column buckling-type instabilities are also possible. This raises interesting questions regarding the interactions of such material instabilities with geometric (or structural) instabilities in bars, plates and shells. The objective of the present work is to study these interactions in the context of the simplest interesting case—mild steel columns whose yield loads are lower than their Euler buckling loads.

The interaction between both types of instabilities in structural members was noted by Haaijer and Thürlimann (1958). They presented a series of experiments of simply supported columns and developed a simple buckling analysis to determine the axial deformation at which buckling occurs. They noted that the experimentally measured strains at buckling showed significant scatter. They attributed the scatter to material property variability between specimens and uncertainty regarding whether one or two Lüders fronts were active in the experiments. We will show that although these are valid reasons for the scatter, they are not the only ones, and that a more sophisticated analysis is necessary to capture the underlying causes.

This study investigates the behavior of columns with Lüders bands. New experiments are first presented that monitor the evolution of the Lüders bands, column deflections and compressive loads for different lengths. Next, finite element simulations using the scheme developed by Shaw and Kyriakides (1998) are used to predict the propagation of the Lüders bands. The purpose of the finite element study is to examine the effect of various parameters on the response and evolution of deformation.

2. Experiments

The column buckling experiments were conducted using a 100 kN (22 kip), uniaxial, servo-hydraulic testing machine equipped with hydraulic grips. The grips enforced essentially clamped boundary conditions at the ends of the column (see Fig. 2). The specimens were cut from 610 mm (24 in.) lengths of 1018 steel, precision ground flat stock bars. The nominal cross-sectional dimensions of the bars were $b = 12.7$ mm by $h = 9.5$ mm (0.500 in. by 0.375 in.). The length of the specimens ranged from 76 to 250 mm (3–10 in.). The bars were stress relieved by the manufacturer. After cutting the specimens to size, they were coated with a brittle coating (StressCoat ST90F) in order to visualize the evolution of the Lüders fronts in the experiments.

The grips of the testing machine were carefully aligned prior to the experiments and then periodically checked in between experiments. The maximum initial misalignment of the grips in the plane of buckling was estimated to be 0.2 mm (0.008 in.) lateral offset and 0.1° angular offset. Due to the grip design, misalignment of the specimen in the perpendicular plane was purely angular and was estimated to be within 0.2°.

Loading of the specimens was applied quasi-statically by prescribing a constant speed for the stroke of the actuator in the testing device. The speed of the actuator was varied depending on the length of the specimen such that the nominal strain rate ($\dot{\Delta}/L$) was 10^{-4} s^{-1}. The compressive displacement (Δ), compressive load (P), and the lateral deflection of the column midspan ($v_{L/2}$, measured using an LVDT) were monitored by a computer-based data acquisition system. A video camera was set up to monitor the plane of

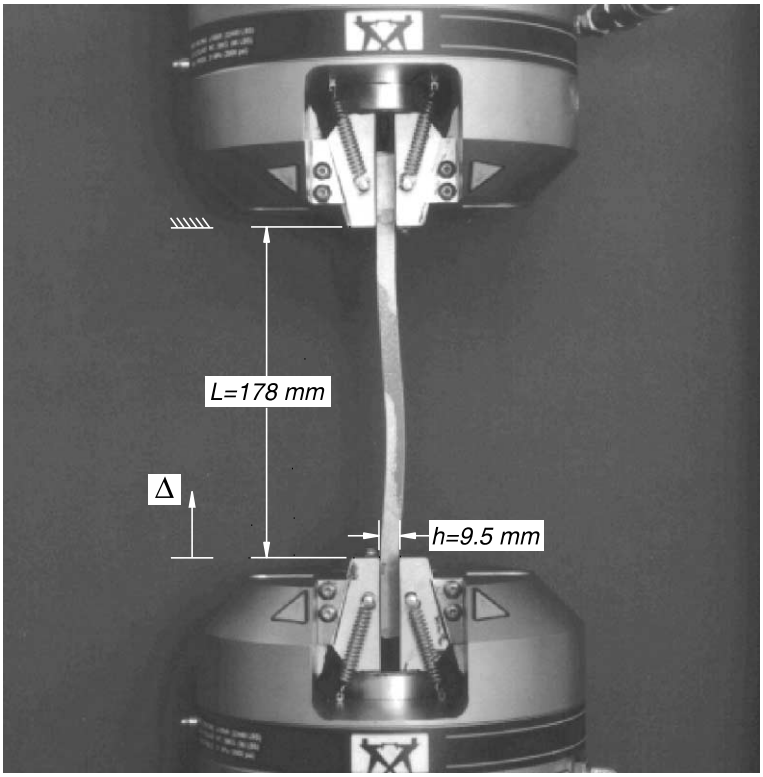

Fig. 2. Photograph of specimen and hydraulic grips.

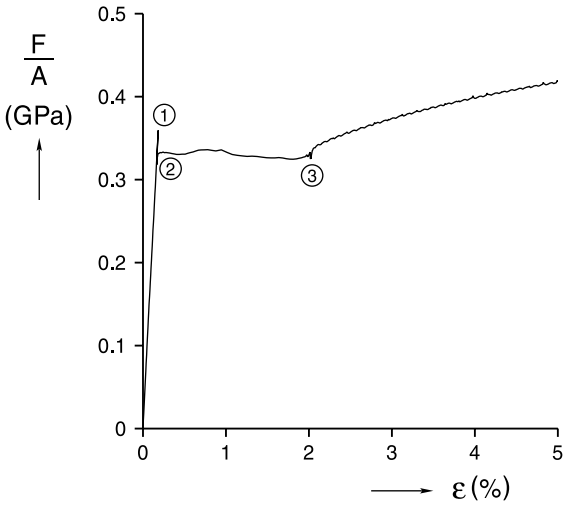

Fig. 3. Engineering stress–strain response of AISI 1018 steel specimen using an extensometer for strain measurement.

buckling of the columns and the evolution of the Lüders bands. A mirror behind the specimen enabled monitoring of the two sides of the column simultaneously.

Tension tests on specimens obtained from the same stock as the compression experiments were used to obtain the stress–strain response of the material. In these tests an extensometer measured the average strain over a 25.4 mm (1 in.) length at the center of the specimen. Fig. 3 shows the measured nominal stress–strain curve corresponding to the plot shown in Fig. 1. Note the cleaner looking nucleation peak in Fig. 3 obtained by using an extensometer. In this test, nucleation occurred outside the extensometer, so elastic unloading to the propagation load was observed at nucleation. The strain remained stationary at ② until the Lüders bands reached the span of the extensometer, and subsequently the measured strain increased to ③. The material properties for the numerical simulations were obtained from the data in Fig. 3. Some variations in the values of upper and lower yield stresses and Lüders strain (in the order of 10%) were noted in the course of the investigation.

Several representative compression experiments are now presented for specimens of different column lengths in order of shortest to longest. Experiments are described in detail for specimens of four different slenderness ratios, L/r, where $r = \sqrt{I/A}$ is the radius of gyration and I is the minimum moment of inertia of the cross-section.

2.1. Experiment 1 ($L/r = 27.7$)

Fig. 4a shows a sequence of images captured from videotape that show the evolution of the deformation of a 76 mm (3 in.) long specimen. The brighter regions of the column are due to the flaking off of the brittle coating caused by the passage of Lüders bands. Although the value of strain that caused the coating to flake off was not determined precisely, it was clearly somewhere within the Lüders strain. The numbers above the images correspond to the instances of the load and displacement history denoted in Fig. 4b and c. The feature in Fig. 4a protruding from the left of the specimen at midspan is the tip of the LVDT used to measure the lateral deflection. Fig. 4b shows the load vs. grip deflection (P–Δ) response while Fig. 4c shows the lateral vs. axial deflection ($v_{L/2}$–Δ) response (deflection to the right corresponds to positive v).

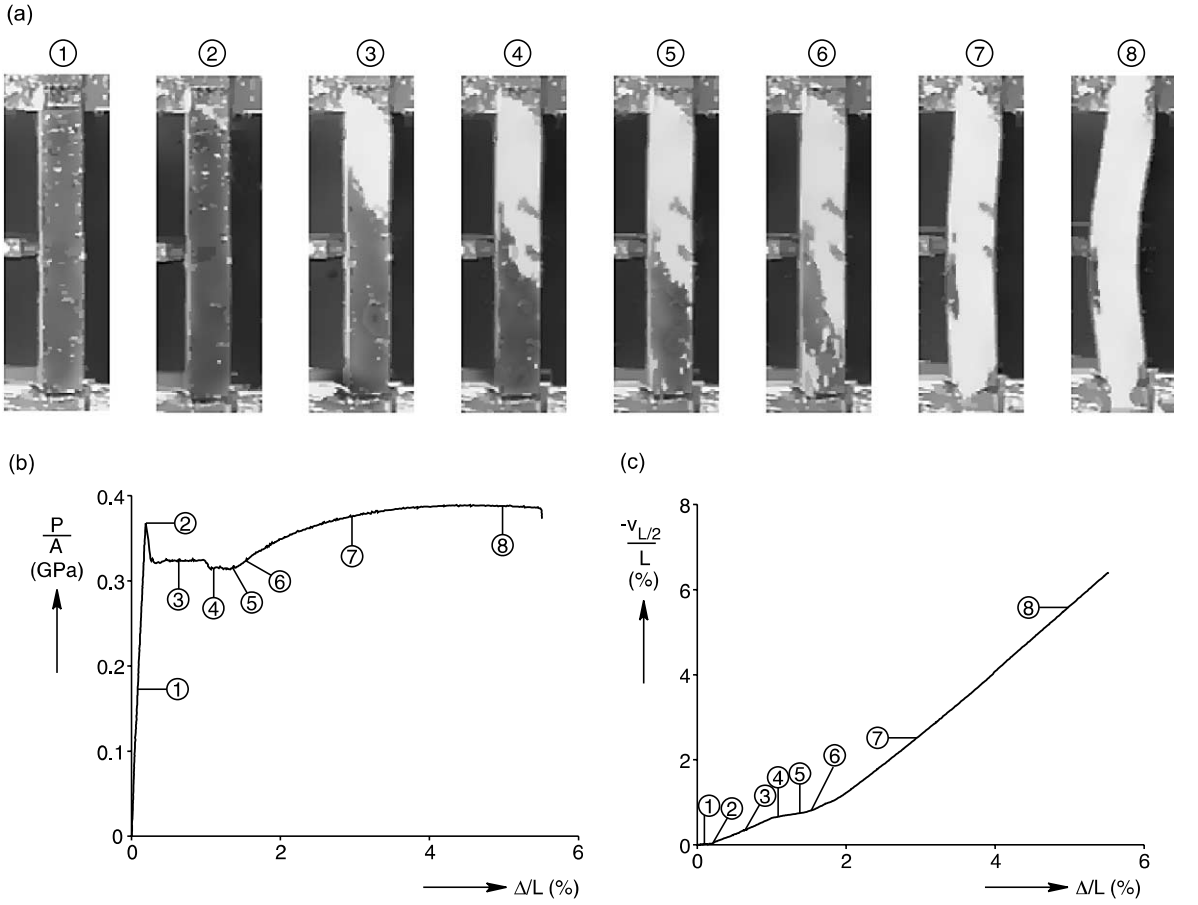

Fig. 4. Response of a 76 mm (3 in.) specimen from Experiment 1 ($L/r = 27.7$): (a) sequence of images showing the evolution of Lüders fronts and column deflections, (b) load-axial deflection, and (c) lateral deflection–axial deflection.

The column was in the elastic range at point ①. The brittle coating covered the length of the column, and the lateral deflection was essentially zero. Image ② in Fig. 4a shows the column at the initial yield point. Yielding occurred first at the top of the column and appears as a small bright inclined band in the image. Looking at the P–Δ curve, note the distinct nucleation peak at yield. The $v_{L/2}$–Δ plot indicates that lateral deflections start at first yield. Image ③ shows a Lüders front propagating downward from the top end. Propagation occurred at nearly constant load as shown in the P–Δ curve. At point ④, the plateau load dropped slightly when yielding started at the lower left corner of the column. [1] Also, note the change in the slope of the $v_{L/2}$–Δ plot at this time. Images ⑤ and ⑥ show that yielding at the lower part of the column occurred in a more diffuse manner, rather than as a clean front. By image ⑥ the yielded regions had merged and the load increased. Further loading caused yielding in most of the specimen as seen in photograph ⑦. Finally, the lateral deflection of the column grew to such an extent that a limit load developed at point ⑧. In the last two photographs, the column displayed a few regions where the brittle coating remained attached.

[1] This is not clearly seen in the image because it started primarily on the backside of the specimen.

On the convex side, this was due to the local reduction and sign change in the compressive stress due to bending. [2] On the concave side, this was due to small stripes of unyielded material. Similar patterns have also been observed in NiTi shape memory alloys (Shaw and Kyriakides, 1998).

From the description above, it is clear that plastic axial strains considerably larger than the Lüders strain can be attained prior to structural collapse. We consider structural collapse to be the point at which the load drops and never recovers. Note, however, that lateral deflections larger than those expected from initial geometric imperfections take place starting at yield. In this case, these deflections during Lüders deformation do not lead to immediate structural collapse. The results to be discussed next pertain to progressively longer specimens that collapse during the propagation of Lüders fronts.

2.2. Experiment 2 ($L/r = 47.4$)

Fig. 5a shows the evolution of deformation in a 130 mm (5 in.) long specimen. The image of the specimen on the left of each frame is the reflection in the mirror placed behind the column. Image ① shows the specimen just before first yield, while image ② shows the nucleation of a Lüders band at the top end (see also the P–Δ curve in Fig. 5b). As compression proceeded, the Lüders front propagated downward as shown in image ③, and a second front nucleated at the bottom of the column as seen most clearly in the mirror image. After the second front started propagating up the column near $\Delta/L = 0.5\%$, a small dip in the P–Δ curve occurred between points ③ and ④. Image ④ shows both fronts propagating towards the center of the specimen. Unlike in the previous example, both fronts were well developed angled bands with nearly opposite sense to one another (oblique angles). At the same time, the lateral deflection of the column increased as shown in Fig. 5c. The load plateau (it actually had a slightly decreasing slope after point ④) extended up to $\Delta/L = 1.3\%$, when the load sharply decreased. The point at which the load clearly started decreasing is considered to be the collapse point. Image ⑤ corresponds to the time when a new yield region nucleated at the right side of the center of the column, caused by the combination of membrane and bending stresses that exceeded the nucleation stress of the material. The new wedge-shaped region was driven primarily by the deflection of the column and propagated along the concave side of the specimen and towards the column axis, as shown in image ⑥. Note that the original fronts remained stationary and that the lateral deflection of the column proceeded at a faster rate after point ⑤. Image ⑦, when the experiment was discontinued, shows that the concave side of the column had completely yielded.

Other experiments showed sequences of events that differed from those presented so far, even for columns of the same length. For example, Fig. 6 shows a comparison of the behavior of two 130 mm (5 in., $L/r = 47.4$) specimens. Fig. 6a shows images of the two specimens at the point of collapse, as indicated in the P–Δ curves in Fig. 6b. Case Ⓐ is the case with oblique fronts discussed above. The specimen in case Ⓑ yielded first at the bottom and displayed only one Lüders front for most of the strain range prior to collapse. Note that the front is somewhat cleaner in the image in the mirror. The front at the top (also seen more clearly in the mirror) initiated just prior to collapse. Note that the Lüders fronts in the image are nearly parallel. The apparent collapse strain for Ⓑ is smaller than for case Ⓐ, but the drop in load in less abrupt for case Ⓑ (continual bending) than for case Ⓐ (sudden appearance of new yielding at midspan). Clearly the different evolution of Lüders patterns, even for the same L/r, can lead to different collapse points. We suspect that relatively minor differences in initial geometric imperfections or load misalignment may be the cause of different events observed.

[2] The behavior of the brittle coating is different in compression and tension. In compression it flakes off at a given strain. In tension it cracks but remains attached unless the strain becomes large.

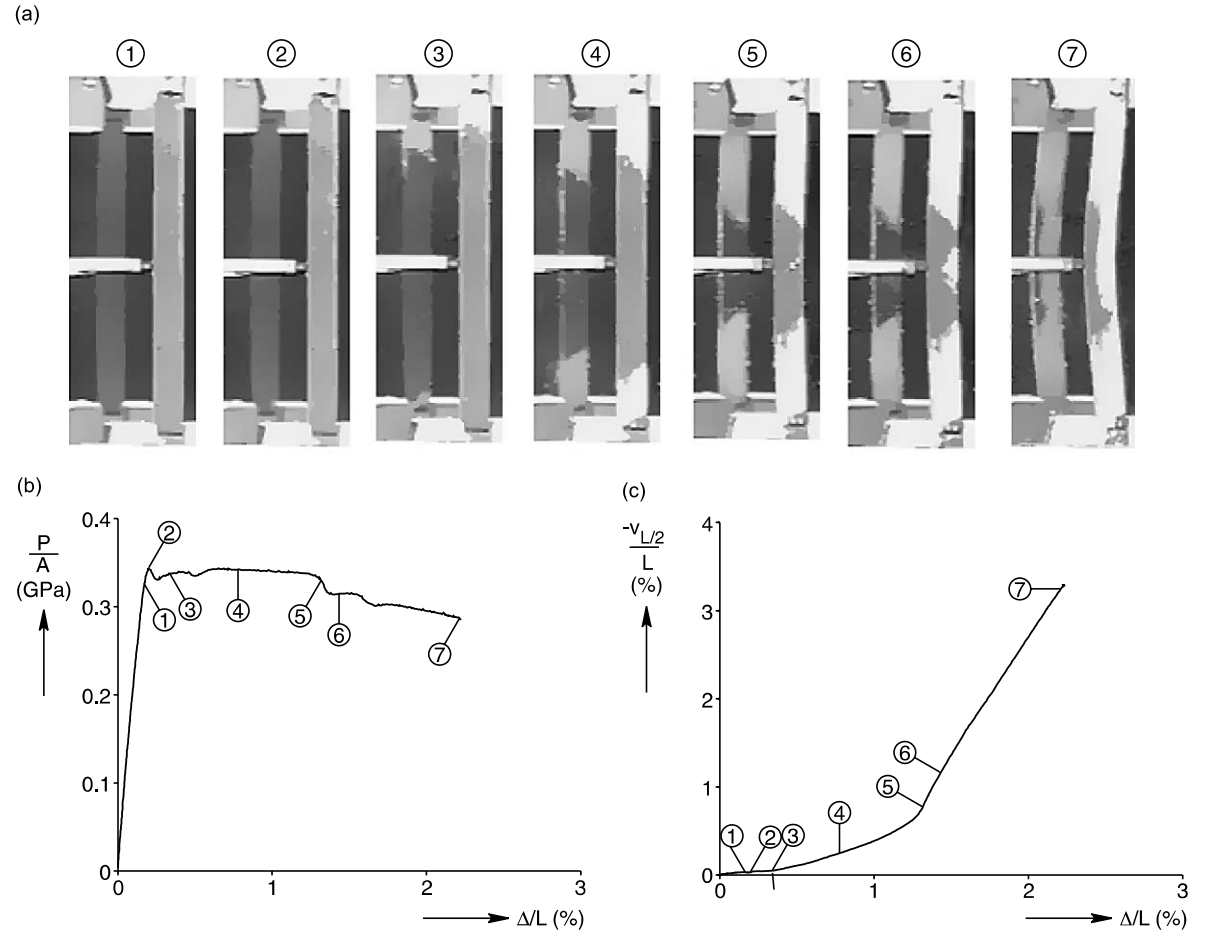

Fig. 5. Response of a 130 mm (5 in.) specimen from Experiment 2 ($L/r = 47.4$): (a) sequence of images showing the evolution of Lüders fronts and column deflections, (b) load-axial deflection, and (c) lateral deflection–axial deflection.

2.3. Experiment 3 ($L/r = 65.6$)

Fig. 7a shows the images captured from an experiment with a 180 mm (7 in.) long specimen. Fig. 7b and c show the P–Δ and $v_{L/2}$–Δ plots, respectively. The column was in the elastic range at point ① and had essentially zero lateral deflection. Image ② shows the column at the yield point. Yielding occurred first at the top of the column just inside of the grips. Looking at the P–Δ plot, note that a nucleation peak did not appear in this experiment. Half of the specimens tested did not exhibit nucleation peaks because the Lüders bands started inside the grips where stress concentrations exist. The $v_{L/2}$–Δ plot indicates that the lateral deflection became noticeably nonzero starting at yield. The lateral deflection first turned positive but changed sign later due to a second front developing at the bottom of the column (see image ③). The two fronts traversed the length of the column from the ends towards the center. Note that the fronts are nearly parallel in this case. The P–Δ response shows a slowly rising load. We consider it likely that the evolving localized deformation causes kinking of the column axis across a Lüders front. This becomes increasingly constrained by the end boundary conditions requiring an increasing load with applied Δ. Note that

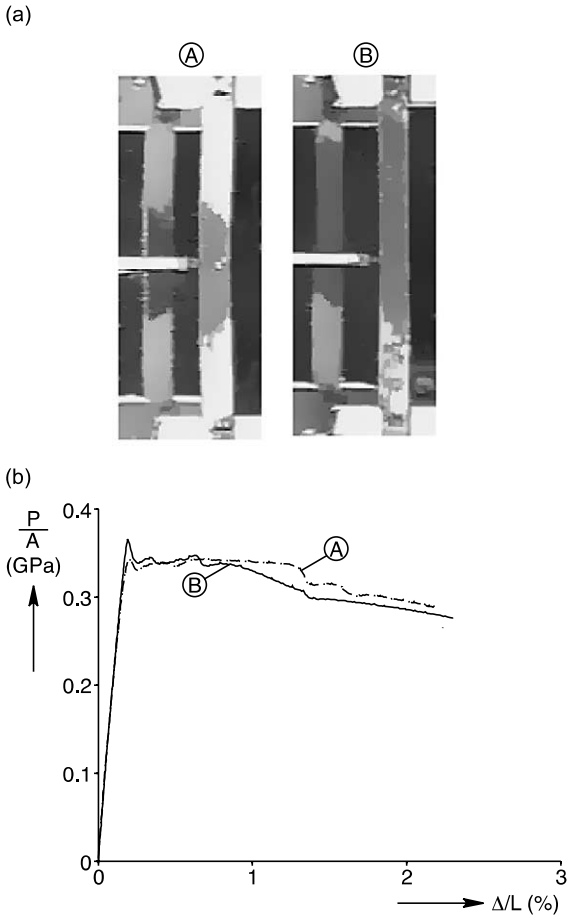

Fig. 6. Comparison of two experiments with specimen lengths of 130 mm (5 in.): (a) images at collapse point and (b) load-axial deflection curves.

depending on the configuration, kinking could also result in less constraint, favoring a load decrease with applied Δ.

We digress here to consider the role of kinking in this structural problem. Shaw and Kyriakides (1998) demonstrated that under tension Lüders-like deformation in fine grained thin strips (mild steel and a NiTi shape memory alloy) under tension developed with the well-known characteristic angle of 54.7° to the axis of loading and had a small kink angle in the plane of the strip (see Fig. 8). Here we have more diffuse fronts due to the low aspect ratio of the specimen cross-section so other angles are possible, but the phenomenon of kinking still exists. Assuming incompressible uniaxial deformations across the front, the kink angle γ can be related to the front angle, Φ, and the uniaxial strain jump, $\Delta\varepsilon$, as

$$\gamma \approx -\frac{3}{4}\Delta\varepsilon \sin(2\Phi)$$

for $\Delta\varepsilon \ll 1$ (see Appendix A). For angles, Φ, between 40° and 60°, which were observed in the experiments, and an axial Lüders strain, $\Delta\varepsilon$, of -0.0186, the kink angle ranges between 0.7° and 0.8°. The kink angle is slight, but it does create a misalignment with the loading axis, thereby causing bending and a possible change in the required load to continue the deformation.

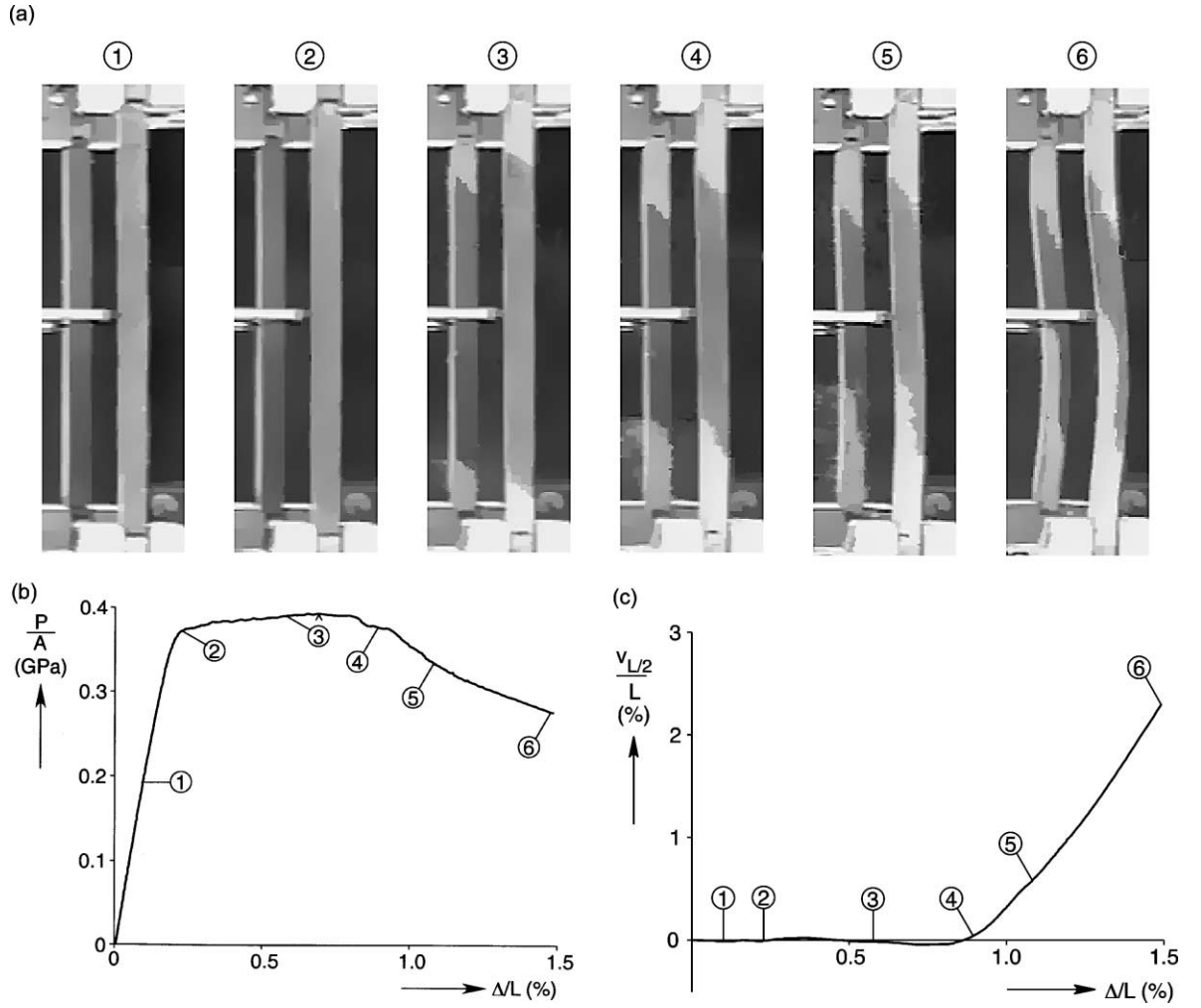

Fig. 7. Response of a 180 mm (7 in.) specimen from Experiment 3 ($L/r = 65.6$): (a) images showing the evolution of Lüders fronts and column deflections, (b) load-axial deflection, and (c) lateral deflection–axial deflection.

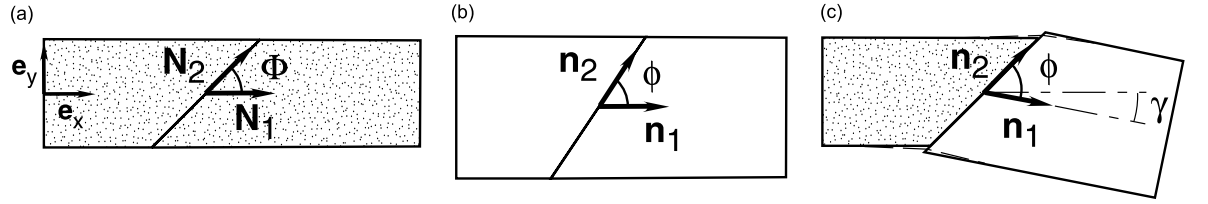

Fig. 8. Kinematics of kinking: (a) elastic, (b) plastic (compression), and (c) transition region showing kink angle, γ.

Continuing our discussion of the experiment, image ④ shows the column just after the collapse point, as shown in the P–Δ plot. The actual maximum in the load occurred, at the point marked by the caret, near end-displacement $\Delta/L = 0.7\%$. A slight 'S' shape in the column is observed in image ④. The cloud in the

mirror near the lower front was due to rapid flaking of brittle coating particles, indicating a rapid propagation of the Lüders deformation in the concave part (left side) of the column. The $v_{L/2}$–Δ graph indicates that the lateral deflection of the column started to rapidly increase. Image ⑤ shows that the lateral deflection of the column increased significantly in the post-collapse regime. In addition, the upper front stopped moving while yielding progressed along the left (concave) side of the column due to the effects of bending. Finally, image ⑥ shows the configuration of the column at the point where the experiment was stopped. Interestingly, the final maximum lateral deflection was near 1/3 of the length from the bottom of the column. The lateral deflection was not symmetric about the midspan, as might be expected in specimens made of materials that deform homogeneously.

2.4. Experiment 4 ($L/r = 83.9$)

Fig. 9 shows images and the load and deflection histories of a 230 mm (9 in.) long specimen. Image ① shows the column in the elastic range. Image ② was taken at first yield, which started at the top of the

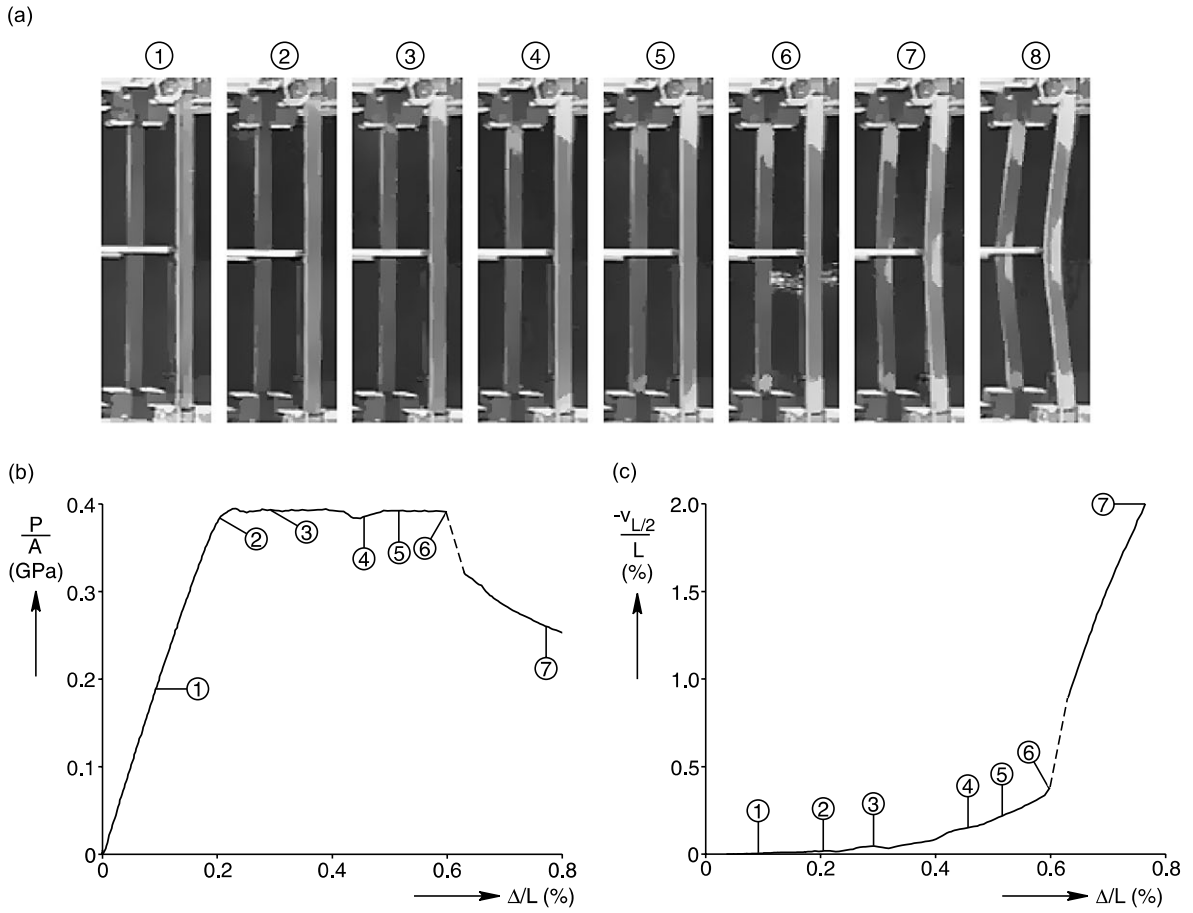

Fig. 9. Response of a 230 mm (9 in.) specimen from Experiment 4 ($L/r = 83.9$): (a) images showing the evolution of Lüders fronts and column deflections, (b) load-axial deflection, and (c) lateral deflection–axial deflection.

column. As in the previous case, the nucleation peak in the P–Δ plot is missing due to stress concentrations at the grips. The lateral deflection remained small until the yield point, but then accelerated after initial yield as seen in the $v_{L/2}$–Δ plot. During approximately the first half of the Lüders plateau, only one front propagated from the top of the specimen as shown in image ③ The temporary load decrease observed in the P–Δ plot just after an end-displacement $\Delta/L = 0.4\%$ corresponded to the appearance of a second front propagating from the lower end of the specimen as shown in photographs ④ and ⑤. It appeared that this front was nucleated in part by a rise in compressive stress on one side of the column due to the increasing lateral deflection. Note that the fronts at the top and bottom of the specimen were initially oblique as in the case of Fig. 5. The evolution of $v_{L/2}$ in the load plateau was monotonic in this case. This indicates that the compressive strain increased on the concave side of the column until the stress locally reached the nucleation value and a new front formed near midspan as shown in photograph ⑥. The nucleation was accompanied by a sudden plume of brittle coating ejected from the nucleation site (see the cloud just below the midspan in image ⑥). At this instant the load decreased abruptly and the lateral deflection jumped to a significantly larger value, as indicated by the dashed lines in Fig. 9b and c. Note that Δ also increased in value suddenly due to the flexibility of the testing machine (Fig. 9b). This sudden jump in deflection seems to indicate that significant elastic energy had been stored in the column to make collapse a dynamic process, rather than the smooth load decrease evident in the other experiments shown. Image ⑦ shows the column in the post-collapse regime, and image ⑧ shows the column at the end of the experiment. It is clear that yielding in the post-collapse regime was dominated by plastic bending of the specimen.

2.5. Discussion

The four examples presented above show most of the range of specimen behaviors observed in this study. Some other experiments, however, showed differences. In four out of 13 specimens collapse occurred with only one front propagating through the specimen. In one case, yielding nucleated at a point within the test section, rather than at the ends.

Fig. 10 shows a summary of the normalized grip displacement at initial yield and collapse as a function of slenderness ratio, L/r, for all 14 experiments conducted in this study. As expected first yield occurred at approximately the same normalized grip displacement in all cases. The three experiments with the shortest lengths developed a limit load after the Lüders fronts had traversed their whole length. Hence, their collapse displacements were much larger than the remainder of the specimens where collapse occurred during partial propagation of Lüders bands. The symbol next to each collapse point indicates the Lüders fronts orientation just prior to collapse, whether as two parallel or oblique fronts or as a single front. One of the $L/r = 72.9$ specimens could not be classified since the Lüders band nucleated at a point within the length of the specimen and at one end, leaving three fronts, so no symbol is shown. The number of data points is relatively small to establish trends with certainty, but some observations can be made:

- In general, the collapse point occurs sooner and sooner after first yield as the columns get more slender, yet the results exhibit scatter as noted by Haaijer and Thürlimann (1958). Specimens of equal slenderness ratio can have significantly different axial displacement at collapse.
- The scatter seems to be at least partially related to the front pattern prior to collapse.
- The pattern seems to suggest that the highest collapse displacement for specimens of equal slenderness ratio tended to occur when the fronts were oblique. The evolution of fronts was, however, more complicated. In some cases, fronts changed their orientation during the loading process.
- The exact details of the boundary conditions at the ends where yielding interacted with the grip interface, which are unknown, may also have an effect on the collapse displacement.

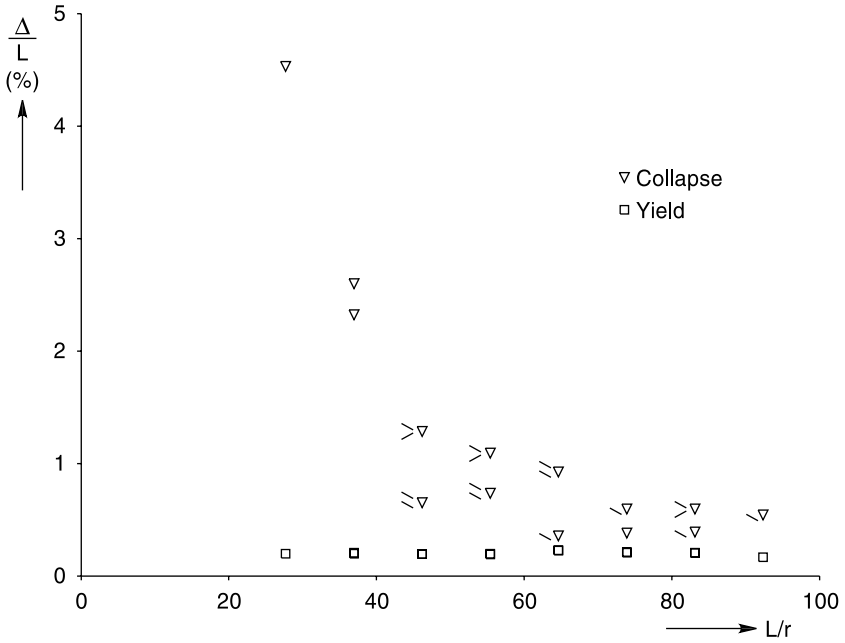

Fig. 10. Yield and collapse deflection for all experiments as a function of slenderness ratio. The lines to the left of each symbol indicate the orientation of the Lüders fronts at collapse.

- The number of fronts and their relative orientation is most likely dependent on the combination of initial imperfections in the specimens and the alignment of the testing machine. The numerical results presented in the next section help to clarify these issues.

3. Finite element simulations

The experiments described above demonstrate interesting interactions between the material-level instability and the structural-level collapse. The phenomena observed in the experiments are rather complex and interactive. Therefore, we now resort to fully three-dimensional finite element simulations to help sort out the details of the evolution of deformation and the origins of the different collapse modes.

The finite element approach of Shaw and Kyriakides (1998) has been shown to successfully capture the three-dimensional deformation fields during the nucleation and propagation of inhomogeneous deformation fields in thin strips under uniaxial tension. It used a conventional J_2 plasticity model that was calibrated to a special trilinear stress–strain curve with a softening intermediate branch. This approach has been used to successfully capture details of transformation fronts that have been observed in experiments of both NiTi shape memory alloys (martensitic transformation) and fine grained mild steels (Lüders bands) under tension. We use a similar approach here to model the material for columns under compression. In the following sections the numerical approach will be outlined and then several finite element analyses will be presented that simulate the experiments discussed previously.

3.1. Numerical approach

The existence of distinctly inhomogeneous deformation fields and a stress plateau during stroke-controlled testing have important implications on material modeling. The engineering stress–strain response

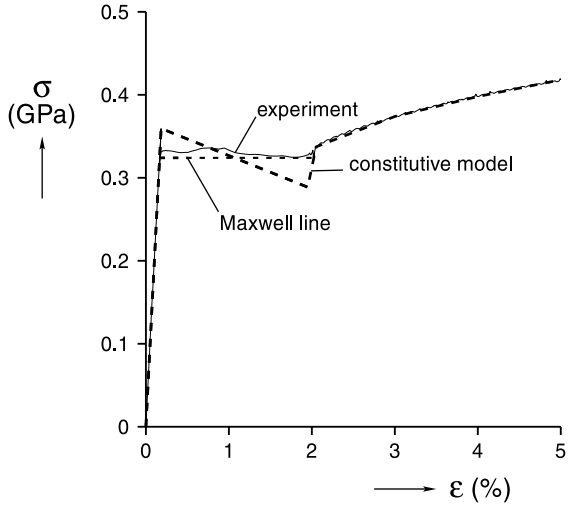

Fig. 11. Engineering stress–strain fit used in finite element simulations.

must be nonmonotonic, since during propagation, multiple strain states are possible for a single axial stress state. Fig. 11 shows a uniaxial curve (dashed line) used to calibrate the constitutive model, consistent with a tensile test of the AISI 1018 carbon steel used in the experiments. A linear softening branch is fitted to the data such that the nucleation stress (359 MPa), Maxwell stress (lower bound of the stress plateau, 324 MPa), and Lüders strain (1.86%) are represented. It should, of course, be recognized that the measured nucleation peak is sensitive to any stress concentrations that exist in the specimen. Therefore, the measured value is actually a lower bound to the true nucleation stress. Nevertheless, in the absence of better information the measured value was used. We use a nonmonotonic uniaxial model to calibrate the rate-independent, finitely deforming J_2 flow rule with isotropic hardening (and softening). We are, of course, aware of the potential concern for pathological mesh sensitivity when softening of the true stress in the continuum-level plasticity model exists, and the reader is referred to the discussion on the subject in Shaw and Kyriakides (1998). Based on a parametric study, the mesh density was chosen fine enough to capture the compression and bending fields relevant to our problem, but not so fine as to allow the appearance of spurious discontinuous deformation gradients since our length scale of interest is the minimum cross-sectional dimension. The number of elements within the bar cross-section was then fixed for all the cases that follow.

The numerical simulations to be presented were performed with the ABAQUS finite element software (HKS, 1999). The grips used in the experiments are not explicitly modeled, with the exception of the last simulation which will be discussed separately. The typical finite element mesh used is shown in Fig. 12. The elements are eight node brick continuum elements, with linear strain interpolation (type C3D8H). The model consists of four elements through the thickness, six elements across the width (not shown), and 32–96 elements along the length. One or more small dents (1–2% of the width) at the ends are used to control the location of first nucleation (indicated by ">" in the following figures). Despite the fact that the forthcoming results all exhibit symmetry about the plane $z = 0$, the entire bar is modeled to ensure no unforeseen structural instability modes are suppressed. The modeled boundary conditions are

$$\begin{aligned} &u(0,y,z) = 0, \quad u(L,y,z) = -\Delta, \\ &v(0,0,z) = 0, \quad v(L,0,z) = 0, \\ &w(0,y,0) = 0, \quad w(L,y,0) = 0, \end{aligned} \tag{1}$$

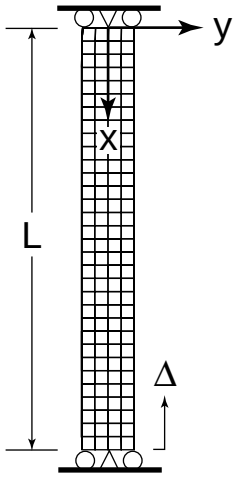

Fig. 12. Typical mesh used in finite element simulations.

with all lateral surfaces traction free. Six simulations are presented below using the same cross-section geometry and same four lengths as in the experiments, starting from shortest to longest.

3.2. Simulation 1 ($L/r = 27.7$)

Fig. 13 shows the axial strain contours (Fig. 13a), mechanical compressive response (Fig. 13b), and midspan deflection (Fig. 13c) for a simulation of a 76 mm (3 in.) long bar. The solid line in Fig. 13b shows the calculated force–deflection response, and the dashed line shows the nonmonotonic constitutive model. Fig. 13a shows the evolution of Lüders deformation, starting in the upper left corner at the upper dent and propagating downward along the length. (Note the time instances shown in the simulation are not the same as in the experiments.) As in the experiment of Fig. 4, a distinct nucleation peak exists in the mechanical response near ①, and then the load remains relatively constant during the Lüders transformation and no buckling-type collapse is seen until after the transformation. Fig. 13c indicates that the bending deflection becomes nonzero starting at time ② and increases slightly through time ④, during which an angled Lüders band is seen in Fig. 13a. At time ⑤ the band becomes more nearly perpendicular to the column axis and the lateral deflection in Fig. 13c levels off until time ⑥. At time ⑦ the Lüders deformation has consumed most of the column and an upturn is seen in both the mechanical response and lateral deflection. Both measures of the deformation compare favorably to that measured in the experiment (Fig. 4b and c) with the only difference being the appearance of a second region of Lüders deformation at the lower end during the experiment near $\Delta/L = 1\%$. This is the point at which the Lüders front becomes less angled in the simulation. Both configurations are mechanisms that tend to minimize the bending deflection. As in the experiment a limit load develops before time ⑧.

3.3. Simulation 2 ($L/r = 47.4$)

Fig. 14 shows the axial strain contours, mechanical compressive response, and midspan deflection for a simulation of a 130 mm (5 in.) long bar. As will be seen in the following two simulations the eventual evolution of deformation is sensitive to the nature of the initial imperfections. The corresponding experiment of Fig. 5 exhibited oblique Lüders fronts. This is simulated by introducing four dents, two at each end, as shown in Fig. 14a. Each dent has a depth of 1% of the width, but the axial extent on the left side is

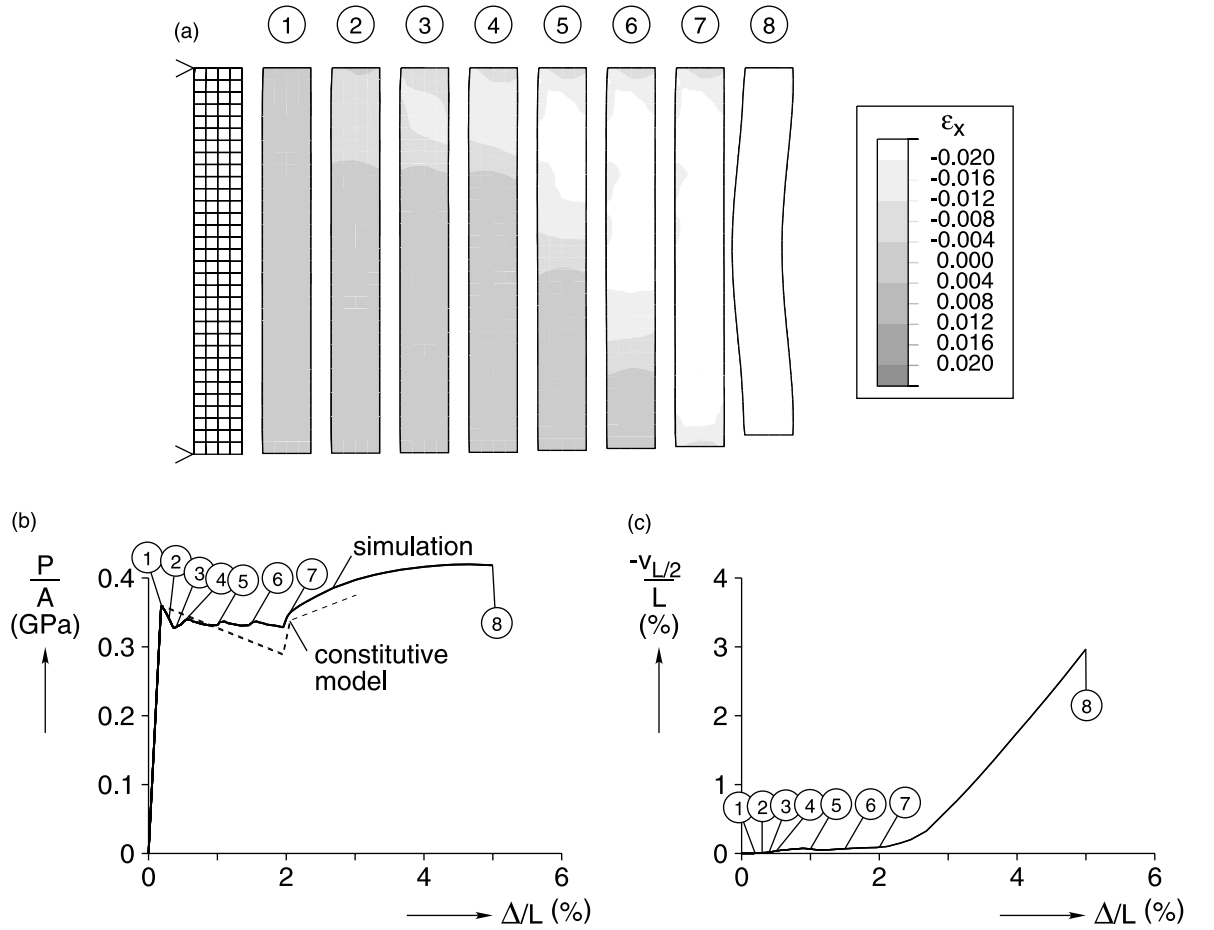

Fig. 13. Simulation 1 ($L/r = 27.7$), 76 mm (3 in.) bar: (a) selected axial strain contours, (b) force–end displacement, and (c) lateral deflection–end displacement.

equal to the width and the axial extent on the right side is equal to one fifth of the width. This results in two angled oblique fronts between times ① and ④. A nucleation peak and then plateau load are seen in the force–displacement response of Fig. 14b, and an upturn in the lateral deflection is observed in Fig. 14c. At time ⑤ (1% average strain) the Lüders strain begins to favor the concave side of the column, resulting in a more pronounced angle of the front in Fig. 14a. Similar to the responses seen in the experiment (Fig. 5b and c) a downturn in the mechanical response and an accelerated lateral deflection are observed at this time. The sequence of axial contours in Fig. 14a are also strikingly similar to the brittle coating images of Fig. 5a.

Fig. 15 shows the lateral deflection (with an inset of the axial strain contours) and rotation of the axis at instant ⑤. The lateral deflection (Fig. 15a) shows a maximum, and nearly constant value, in the midsection that is elastic. It resembles the start of a mode 1 buckling mode. The rotation angle (Fig. 15b) distribution is piecewise constant over each element in the mesh due to the linear interpolation. It shows a jump in the rotation angle of about 0.6° across each front, which is reasonably consistent with the kinking analysis given previously. This suggests that kinking plays the role of an imperfection that may bias the deflection towards or away from eventual structural collapse.

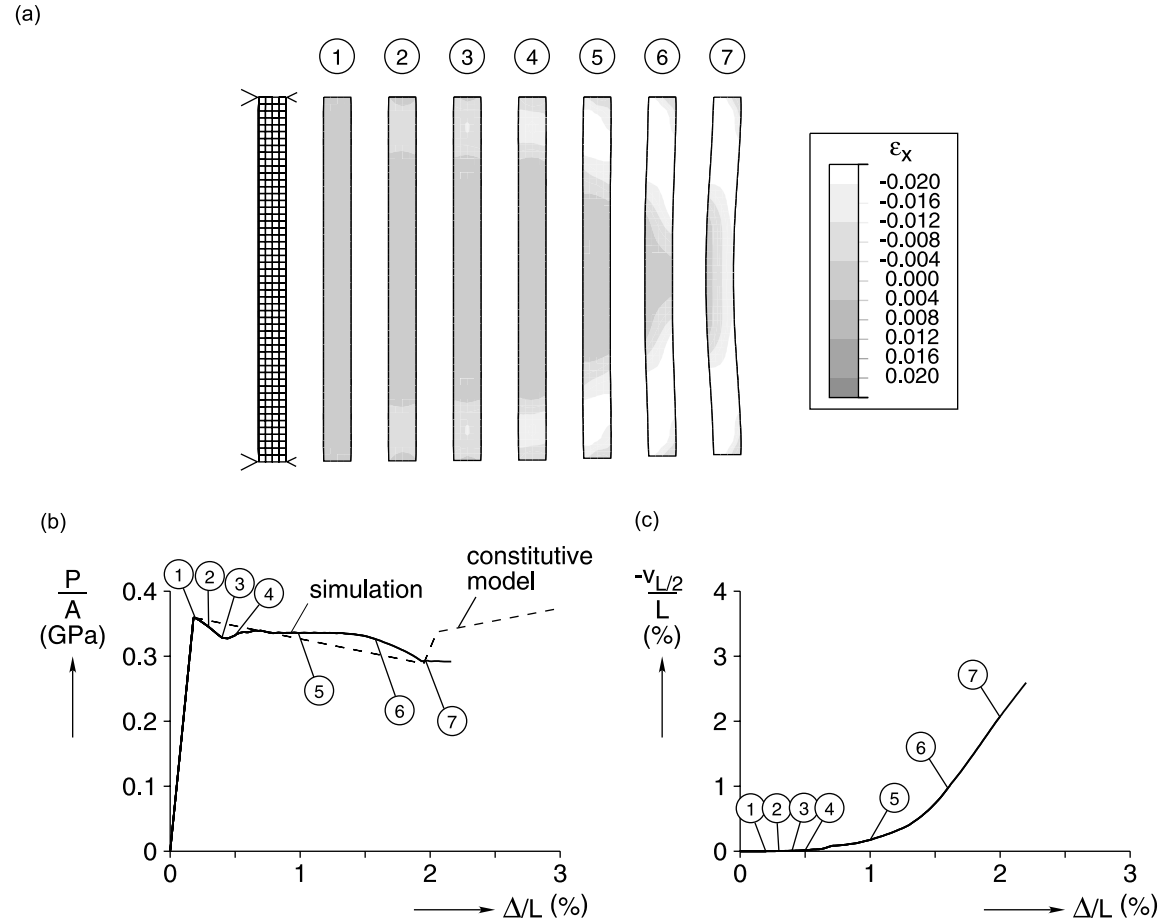

Fig. 14. Simulation 2 ($L/r = 47.4$), 130 mm (5 in.) bar: (a) selected axial strain contours, (b) force–end displacement, and (c) lateral deflection–end displacement.

3.4. Simulation 3 ($L/r = 65.6$)

Fig. 16 shows the case of a 180 mm (7 in.) long bar with two imperfections placed on opposite ends and opposite sides of the column. This arrangement of imperfections results in parallel fronts as shown in Fig. 16a. The resulting lateral deflection at the midspan is identically zero, so the corresponding figure is not shown. The force–deflection response in Fig. 16b shows the same type of nucleation peak as before (it is missing in the corresponding experiment of Fig. 7 due to the Lüders bands starting within the grips) and then a slightly rising load plateau during times ③ and ④. Between times ④ and ⑤ the load takes a downturn and plastic bending in a mode 2 buckling shape (S-shape) becomes evident. Further shortening occurs at a progressively lower load while more pronounced bending occurs in this anti-symmetric mode. The events from ① and ④ are quite similar between the simulation and the experiment. Subsequently, the simulation maintains perfect anti-symmetry about the midspan, yet the deformation in the experiment lost any such symmetry as the lower front traversed faster than the upper one. This is, perhaps, not surprising since any misalignment in practice will allow the deformation to proceed towards a mode 1 shape. Although not

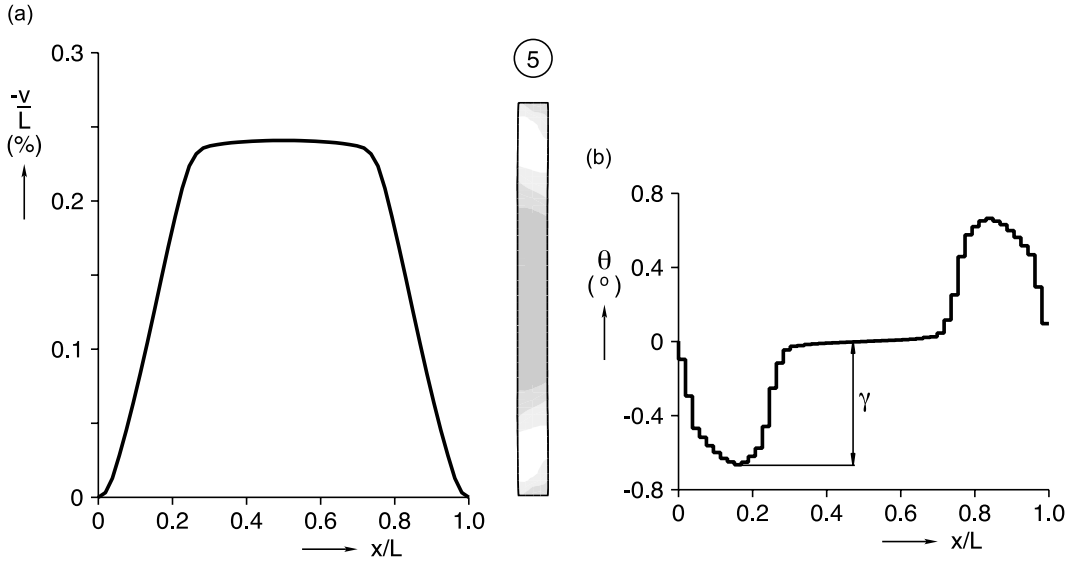

Fig. 15. Simulation 2 at point ⑤: (a) midaxis lateral displacement and (b) midaxis rotation.

shown, a quite similar response was calculated for an undented column with one end initially displaced laterally by 0.127 mm (0.005 in.), which is within the range of the misalignment seen in the experiments.

3.5. Simulation 4 ($L/r = 65.6$)

Fig. 17 also shows the case of a 180 mm (7 in.) long bar but with the two imperfections placed on the same side of the column. Unlike the previous case, collapse is predicted as soon as yielding occurs. Lüders fronts do not get a chance to propagate. Instead, plastic hinges are generated at the ends and at the midspan, resulting in a mode 1 like buckle. It is interesting that the slight change in imperfection pattern from the previous case makes such a dramatic difference in the deformation history and collapse mode. Also not shown, a similar response is calculated for a column without any dents but with one end rotated by 0.6° before being compressed. It appears that any imperfection or nudge in the direction of the first buckling mode favors an immediate collapse. By contrast, the previously presented simulation and the experiment suggest that imperfections or loading favoring a higher buckling mode can result in that mode being temporarily locked in by plasticity, thereby delaying the eventual collapse.

3.6. Simulation 5 ($L/r = 83.9$)

Fig. 18 shows the case of a 230 mm (9 in.) long bar with the same four imperfections as used in Simulation 2 (Fig. 14). The collapse is immediate upon first yield with a similar deformation mode as in Simulation 4 (Fig. 17). The rate of collapse is more severe than the previous simulation, however, due to the slenderness of the column. Unfortunately, this simulation exhibits collapse well before that of the experiment in Fig. 9. Several other imperfection patterns and loading variations were attempted, but the collapse into a mode 1 like shape was immediate in all cases and Lüders fronts did not propagate.

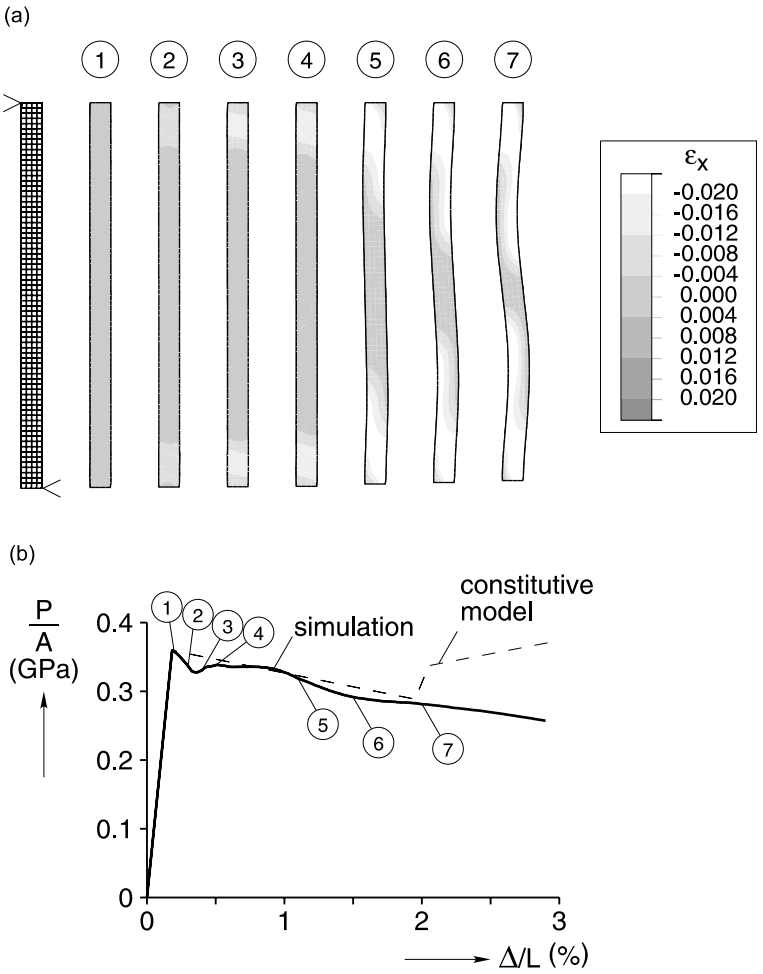

Fig. 16. Simulation 3 ($L/r = 65.6$), 180 mm (7 in.) bar with asymmetric imperfections: (a) force–end displacement and (b) selected axial strain contours.

3.7. Simulation 6 ($L/r = 83.9$)

There are two possible causes of the premature collapse seen in Simulation 5, either the modeled nucleation peak was too small or no credit was taken for the actual boundary conditions at the grips. The remedy involves preventing plastic collapse at the midspan which is due to excessive bending stress caused by kinking at the nucleation sites at the ends. Modeling a larger nucleation peak would increase the required bending stress to form a plastic hinge at the midspan; however, we had no basis for choosing a specific higher value for the nucleation stress. An alternative approach, which is adopted here, is to include the effects of the grips. We suspect that giving a Lüders front a sort of running start from within the grips prevents large bending stresses from occurring at the midspan. A simple representation of the grip was added to the model for this simulation. The finite element mesh used is shown in Fig. 19 for the case of a 230 mm (9 in.) long bar, but now the clamping pressure of the grips is included. The same element type and

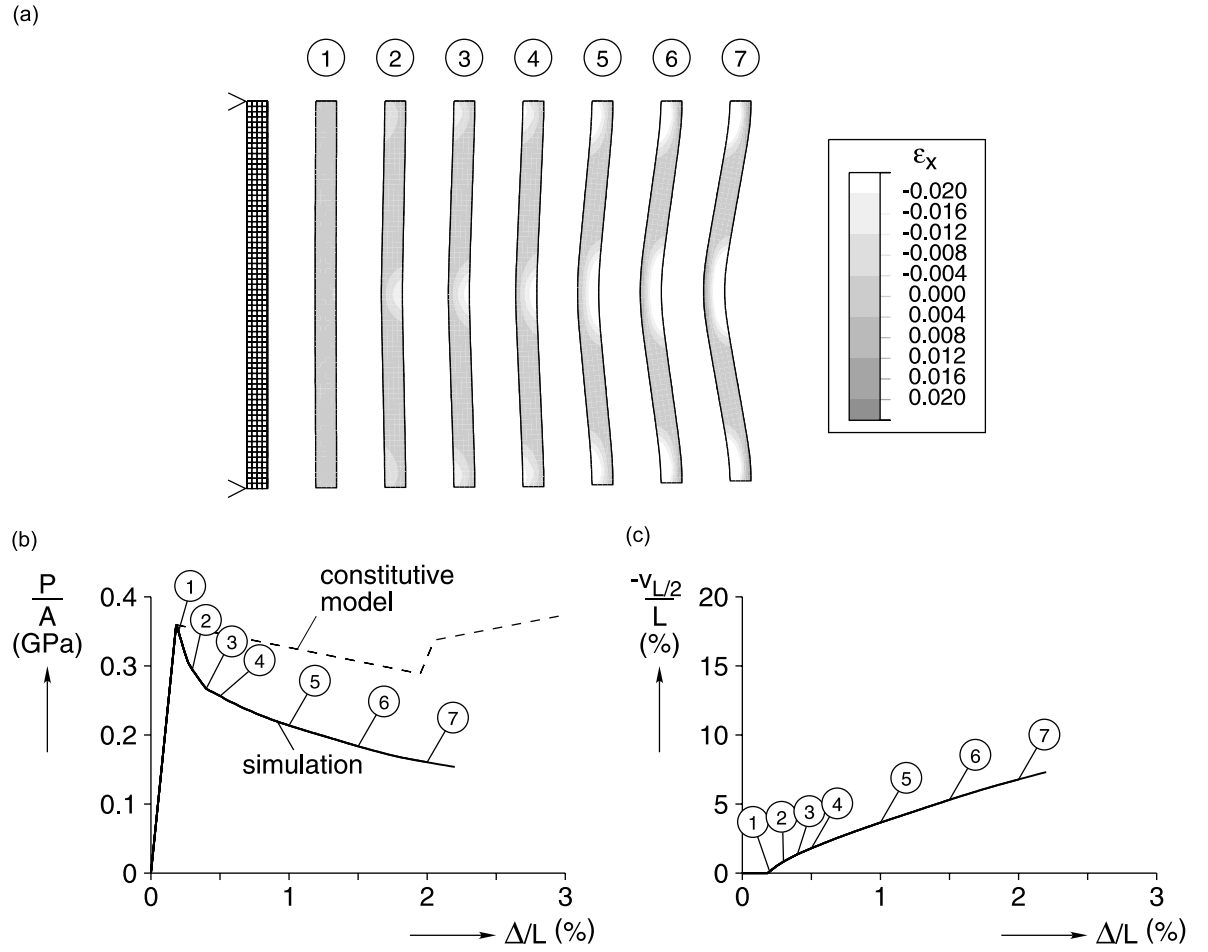

Fig. 17. Simulation 4 ($L/r = 65.6$), 180 mm (7 in.) bar with symmetric imperfections: (a) selected axial strain contours, (b) force–end displacement, and (c) lateral deflection–end displacement.

number of elements through the thickness and across the width are used as in the prior simulations, but an additional 2 in. of length are added to the top and bottom to be clamped within the grips. Small bulges are introduced within each grip region to act as stress concentrations to control the location of first nucleation. Fig. 20a shows the location of the bulges with a ">". The bulges are 1% and 0.5% of the thickness, located in the top and bottom grip regions, respectively. The boundary conditions are

$$
\begin{aligned}
&u(-L_g, \pm h/2, z) = 0, \quad u(0, \pm h/2, z) = 0,\\
&u(L, \pm h/2, z) = -\Delta, \quad u(L + L_g, \pm h/2, z) = -\Delta,\\
&w(-L_g, 0, 0) = 0, \quad w(L + L_g, 0, 0) = 0,
\end{aligned}
$$

$$
v(x, \pm h/2, z) = \mp v_g \quad \text{for} \begin{cases} -L_g \leqslant x \leqslant 0 \\ L \leqslant x \leqslant L + L_g \end{cases} \tag{2}
$$

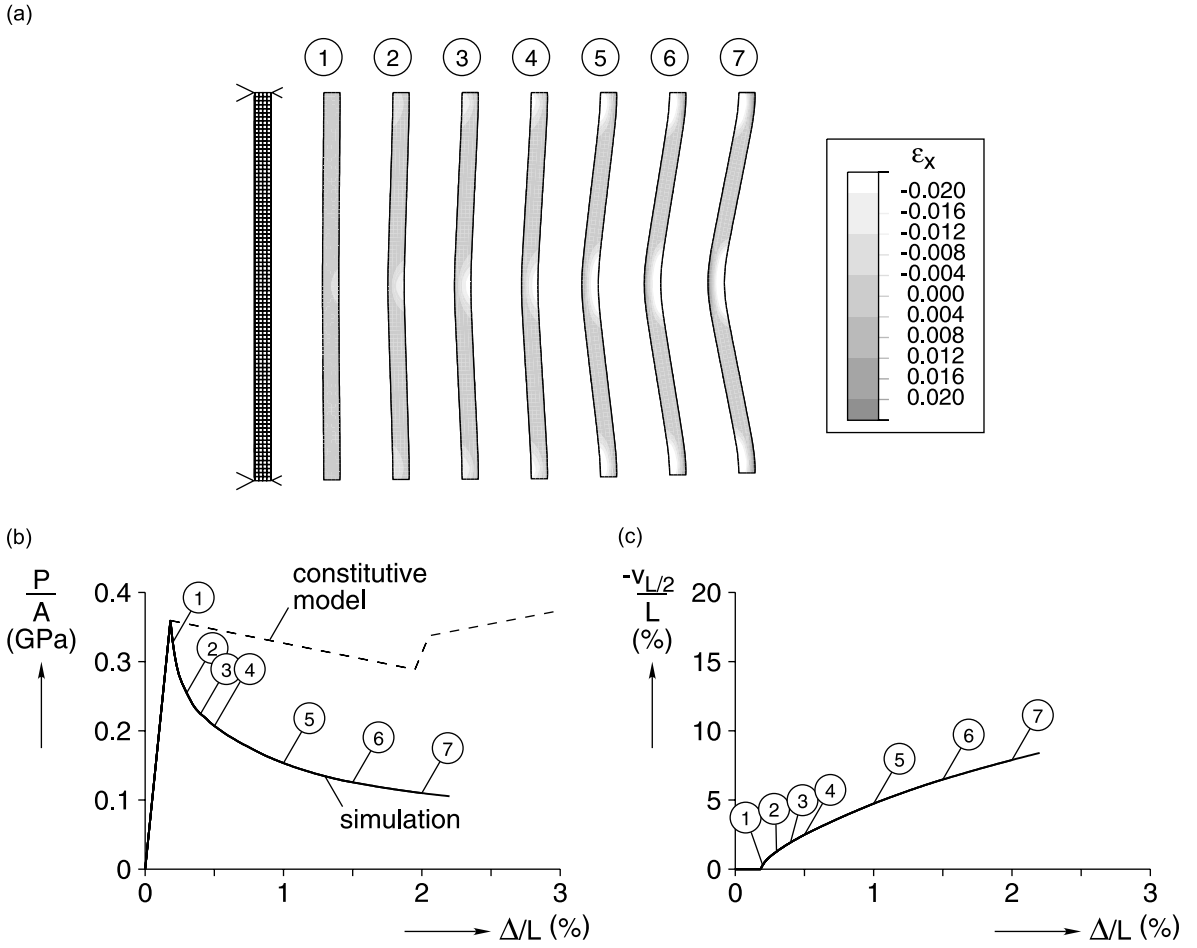

Fig. 18. Simulation 5 ($L/r = 83.9$), 230 mm (9 in.) bar with symmetric imperfections: (a) selected axial strain contours, (b) force–end displacement, and (c) lateral deflection–end displacement.

with the other surfaces traction free, and where v_g is the initial lateral clamping displacement, chosen to produce slight yield within the grip, $2v_g/h = -0.24\%$ lateral strain.

The results are shown in Fig. 20. The simulated grips result in a single front that nucleates partially within the top grip, and propagates down the length between ③ and ⑦, as shown in Fig. 20a. The nucleation peak (① in Fig. 20b) is slightly reduced due to the stress concentration occurring in the grip, but is not eliminated as was in Figs. 7b and 9b. The front remains relatively perpendicular to the column axis until ⑥, after which it becomes somewhat angled. Between ⑥ and ⑦ the specimen begins to collapse. This leads to the sudden appearance of yielding at the lower grip and a sudden drop in load. This behavior demonstrates the stable propagation of Lüders bands observed in long specimens. In addition, the severe drop in load after ⑥ and the appearance of a detached yield region near midspan somewhat mimics the dynamic collapse observed in Experiment 4 (Fig. 9).

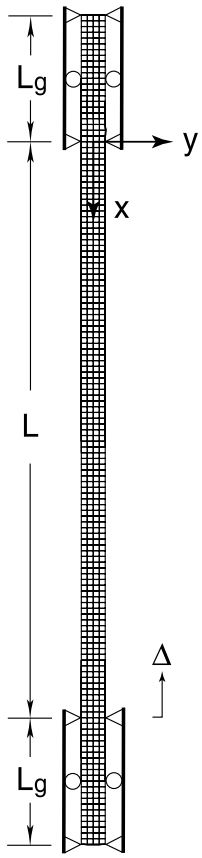

Fig. 19. Finite element mesh and boundary conditions to model the effects of grips in Simulation 6.

4. Summary and conclusions

Experiments and simulations were presented for compression of mild steel bars that exhibit Lüders bands prior to collapse. The study included an investigation of bars having the same cross-section but several different lengths. The mechanical response in the experiments were monitored through measurements of axial load, axial and lateral displacements, and full field imaging of a brittle coating. Interesting interactions were observed between the localized deformation due to the material-level instabilities and the structural, or global, collapse of the bars. The numerical simulations used a constitutive model with an unstable branch similar to the approach of Shaw and Kyriakides (1998), and overall, showed good agreement with the experiments. The following points are worth emphasizing.

- As expected, the average collapse strain tended to decrease as the slenderness of the specimen was increased. Interestingly, in most cases the bars collapsed well after first yield. The collapse strain, however, exhibited significant scatter even for the same specimen geometry (as noted in Haaijer and Thürlimann (1958)).

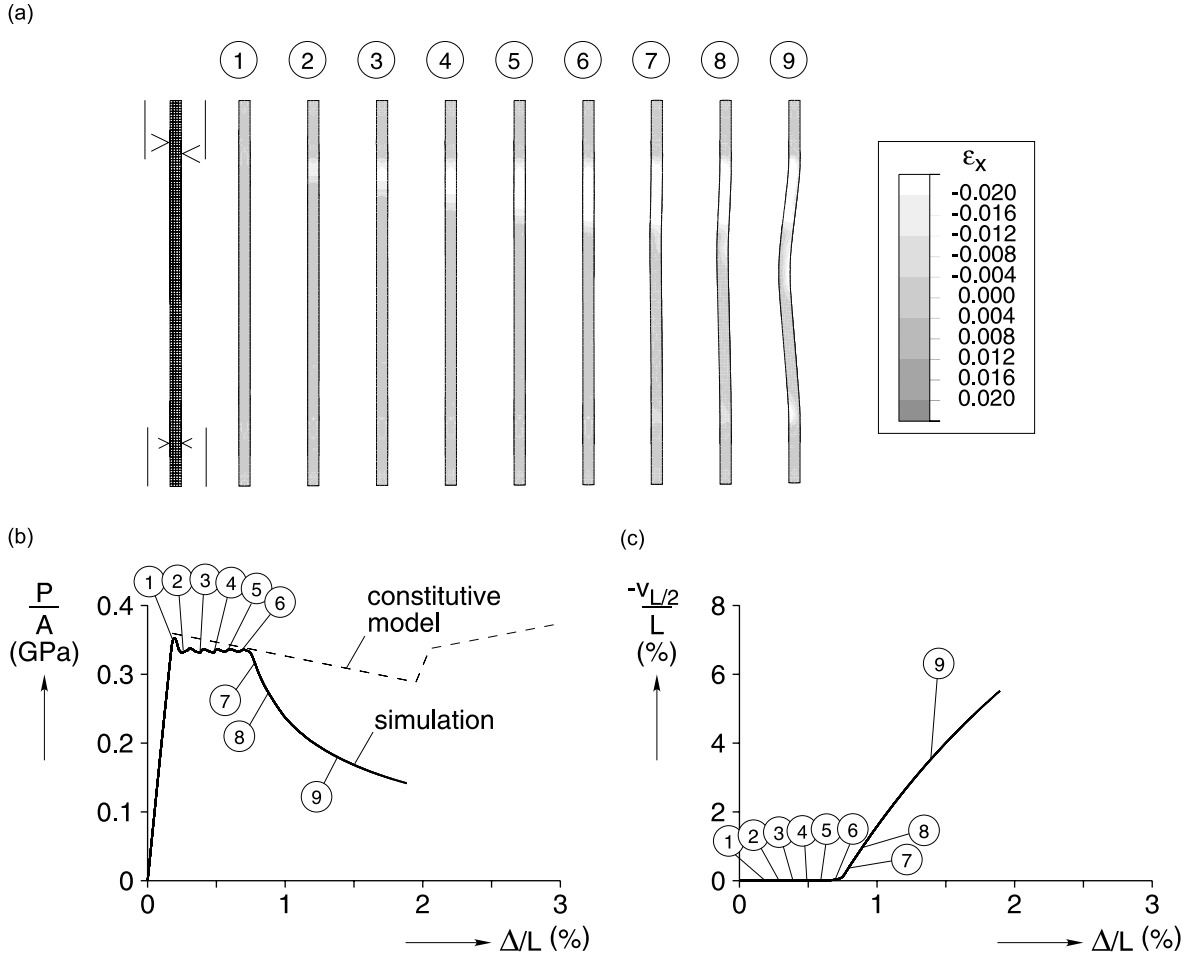

Fig. 20. Simulation 6 ($L/r = 83.9$), 230 mm (9 in.) bar with grips: (a) selected axial strain contours, (b) force–end displacement, and (c) lateral deflection–end displacement.

- The scatter seemed to be at least partially related to the Lüders front pattern prior to collapse. Considering the numerical cases studied, we consider the evolution of the front pattern to be strongly sensitive to the nature of the initial imperfections and loading misalignments.
- Kinking of the column axis due to angled fronts, although a somewhat diffuse phenomenon for the aspect ratio of the cross-section used, seemed to play a role in the collapse modes observed. Numerical results suggest that front patterns creating bending deflections akin to higher order buckling modes could be temporarily locked in by plasticity, thereby delaying collapse until well past initial yield. In both the experiments and numerical simulations, shorter specimens collapsed gradually while longer specimens displayed a more dynamic collapse.
- Numerical simulations showed that the symmetry of imperfections and/or initial loading misalignment have a dramatic effect on the evolution of deformation and subsequent collapse. A judicious choice of imperfections was sufficient to achieve good agreement with the experiments for the three shorter length columns studied. Modeling of more realistic grip-like boundary conditions was necessary to capture the

events seen in the experiment on the longest column simulated. Overall, the numerical study of various initial imperfections provided insight into the origins of the scatter in the experimental data.

Acknowledgements

The financial support of the National Science Foundation (E. Corona, J. Shaw), the US Air Force Office of Scientific Research (J. Shaw), the University of Michigan Arnold M. Kuethe Fellowship (M. Iadicola), and the University of Notre Dame (E. Corona) are acknowledged with sincere thanks. Special thanks to Prof. C. Calladine are in order for drawing our attention to the paper by Haaijer and Thürlimann (1958).

Appendix A

Fig. 8c shows a schematic of an angled transformation front across the width of a uniaxial specimen with untransformed material to the left and transformed material to the right. The reference front angle, Φ (Fig. 8a), is defined by $\mathbf{N}_1$ and $\mathbf{N}_2$ as

$$\cos\Phi = \mathbf{N}_1 \cdot \mathbf{N}_2 \quad \text{where, } \mathbf{N}_1 = 1\mathbf{e}_x \text{ and } \mathbf{N}_2 = \cos\Phi\mathbf{e}_x + \sin\Phi\mathbf{e}_y.$$

The convected front angle, ϕ (Fig. 8b), is given by

$$\cos\phi = \mathbf{n}_1 \cdot \mathbf{n}_2 \text{ where, } \mathbf{n}_1 = \frac{\mathbf{F}\cdot\mathbf{N}_1}{\|\mathbf{F}\cdot\mathbf{N}_1\|} \text{ and } \mathbf{n}_2 = \frac{\mathbf{F}\cdot\mathbf{N}_2}{\|\mathbf{F}\cdot\mathbf{N}_2\|},$$

and $\mathbf{F}$ is the relative deformation gradient. Thus,

$$\mathbf{n}_1 \cdot \mathbf{n}_2 = \frac{\mathbf{N}_1\cdot\mathbf{C}\cdot\mathbf{N}_2}{\sqrt{\mathbf{N}_1\cdot\mathbf{C}\cdot\mathbf{N}_1}\sqrt{\mathbf{N}_2\cdot\mathbf{C}\cdot\mathbf{N}_2}}.$$

Under uniaxial, incompressible deformation the right Cauchy–Green tensor $\mathbf{C} = \mathbf{F}^{\mathrm{T}}\cdot\mathbf{F}$ is

$$\mathbf{C} = \lambda^2\mathbf{e}_x\otimes\mathbf{e}_x + \frac{1}{\lambda}\mathbf{e}_y\otimes\mathbf{e}_y + \frac{1}{\lambda}\mathbf{e}_z\otimes\mathbf{e}_z,$$

where λ is the uniaxial stretch ratio across the front. It is well known that a front angle of $\Phi = 54.7°$ is an inextensional direction for thin strips. We have not, however, imposed such a condition, since the aspect ratio of the specimen cross-section is relatively low (3:4) and the fronts are somewhat diffuse (see dashed outline in Fig. 8c). Consequently, other front angles are possible. The finite rotation to align $\mathbf{N}_2$ with $\mathbf{n}_2$ is the kink angle, γ (Fig. 8c), given by

$$\gamma = \cos^{-1}\left[\frac{1}{\sqrt{1+\frac{\tan^2\Phi}{(1+\Delta\varepsilon)^3}}}\right] - \Phi,$$

where $\Delta\varepsilon$ is the uniaxial engineering strain jump across the front. Since γ is a small angle and $\Delta\varepsilon \ll 1$, this equation can be linearized as

$$\gamma \approx -\frac{3}{4}\Delta\varepsilon\sin(2\Phi).$$

References

Butler, J.F., 1962. Lüders front propagation in low carbon steels. Journal of the Mechanics and Physics of Solids 10, 313–334.
Haaijer, G., Thürlimann, B., 1958. On inelastic buckling of steel. ASCE Journal of the Engineering Mechanics Division 84, 1581-1–1581-48.
Hall, E.O., 1970. Yield Point Phenomena in Metals and Alloys. Macmillan, NY.
HKS, 1999. ABAQUS Manual, version 5.8.
Kyriakides, S., Miller, J.E., 2000. On the propagation of Luders bands in steel strips. Journal of Applied Mechanics 67 (4), 645–654.
Shaw, J.A., Kyriakides, S., 1998. Initiation and propagation of localized deformation in elasto-plastic strips under uniaxial tension. International Journal of Plasticity 13, 837–871.